

Switching Independent Vector Analysis and Its Extension to Blind and Spatially Guided Convolutional Beamforming Algorithm

Tomohiro Nakatani, *Fellow, IEEE*, Rintaro Ikeshita, *Member, IEEE*, Keisuke Kinoshita, *Senior Member, IEEE*, Hiroshi Sawada, *Fellow, IEEE*, Naoyuki Kamo, Shoko Araki, *Senior Member, IEEE*,

Abstract—This paper develops a framework that can perform denoising, dereverberation, and source separation accurately by using a relatively small number of microphones. It has been empirically confirmed that Independent Vector Analysis (IVA) can blindly separate N sources from their sound mixture even with diffuse noise when a sufficiently large number ($= M$) of microphones are available (i.e., $M \gg N$). However, the estimation accuracy seriously degrades as the number of microphones, or more specifically $M - N$ (≥ 0), decreases. To overcome this limitation of IVA, we propose switching IVA (swIVA) in this paper. With swIVA, time frames of an observed signal with time-varying characteristics are clustered into several groups, each of which can be well handled by IVA using a small number of microphones, and thus accurate estimation can be achieved by applying IVA individually to each of the groups. Conventionally, a switching mechanism was introduced into Minimum-Variance Distortionless Response (MVDR) beamformer; however, no blind source separation algorithms with a switching mechanism have been successfully developed until this paper. In order to incorporate dereverberation capability, this paper further extends swIVA to blind Convolutional beamforming algorithm (swCIVA). It integrates swIVA and switching Weighted Prediction Error-based dereverberation (swWPE) in a jointly optimal way. With swCIVA, two different time-varying characteristics of an observed signal are captured, respectively, for dereverberation and source separation to achieve effective estimation. We show that both swIVA and swCIVA can be optimized effectively based on blind signal processing, and that their performance can be further improved using a spatial guide for the initialization. Experiments show that the both proposed methods largely outperform conventional IVA and its Convolutional beamforming extension (CIVA) in terms of objective signal quality and automatic speech recognition scores when using a relatively small number of microphones.

Index Terms—Source separation, dereverberation, microphone array, switching system, blind signal processing

I. INTRODUCTION

When a speech signal is captured by distant microphones, e.g., in a conference room, it often contains such interference signals as reverberation, diffuse noise, and voices from extraneous speakers. They all reduce the intelligibility of the captured speech and often cause serious degradation in many speech applications, such as hands-free teleconferencing and Automatic Speech Recognition (ASR) [1].

Blind source separation (BSS) has been actively studied to minimize the aforementioned detrimental effects in acquired signals. It separates a sound mixture captured by a

microphone array into given number of sources based on general statistical characteristics of sources, not relying on prior knowledge of the individual sources or the recording conditions. A number of techniques have been developed for BSS, including Independent Component Analysis (ICA) [2], [3], Independent Vector Analysis (IVA) [4]–[6], Full-rank spatial Covariance Analysis (FCA) [7], [8], and spatial clustering-based masking and beamforming [9]–[11]. Among them, IVA separates sources as mutually independent vectors, each of which corresponds to each source’s full-band complex spectra in the Short-Time Fourier Transform (STFT) domain. Thanks to this mechanism, IVA can solve the well-known frequency permutation problem of BSS [9] without any post processing for it. In addition, IVA assumes a determined condition for BSS, i.e., the number of sources N is equal to that of microphones M . Under this assumption and when we have more microphones than sources, i.e., $M > N$, it is empirically confirmed that IVA can separate N sources and $M - N$ noise components from a sound mixture with stationary diffuse noise [12], [13]. Based on this capability, Independent Vector Extraction (IVE) has been recently proposed as a variation of IVA that can extract only N sources from such a noisy mixture in a computationally efficient way [14]–[16].

For performing blind dereverberation (BD), Weighted Prediction Error-based dereverberation (WPE) has been shown effective [17]–[19]. It uses a Multi-Channel Linear Prediction (MCLP) filter to perform dereverberation, and optimizes the filter based on the Maximum Likelihood (ML) estimation. WPE can improve various signal processing techniques, e.g., beamforming [20], [21], ASR [22], [23], and speaker recognition/diarization [24], [25], to name a few, by using it as a preprocessing in far-field signal capturing situations.

Convolutional BeamFormers (CBFs) [26]–[33] have also been studied to jointly perform BSS and BD. A CBF is defined in this paper as an STFT-domain filter that spans more than one time frame. It can be factorized into a separation matrix and an MCLP filter, and can perform BSS and BD in a jointly optimal way by integrating IVA and WPE [28], [30], [34]. This paper refers to this type of CBF optimization algorithm as *blind Convolutional beamforming algorithm with IVA (CIVA)*. Computationally efficient optimization techniques have been developed for CIVA without the factorization [32], [35], or with it [34]. An extension that incorporates IVE into CIVA has also been proposed [36]–[38]. It works very well to jointly perform denoising, dereverberation, and source

T. Nakatani, R. Ikeshita, H. Sawada, K. Kinoshita, N. Kamo, and S. Araki are with NTT Corporation.

Manuscript received July 1, 2021; revised XXXX XX, 2020.

TABLE I
TAXONOMY OF ALGORITHMS FOR DEREVERBERATION (DR),
BEAMFORMING (BF), AND CONVOLUTIONAL BEAMFORMING (CBF)

DR/BF/ CBF	Switch	With ATF	Blind
DR	-	-	WPE [17]–[19]
BF	-	MVDR BF [39]	IVA [4]–[6]
CBF	-	wMPDR CBF [40], [41]	CIVA [32], [34]
DR	✓	-	swWPE [42]
BF	✓	MVDR swBF [43]	swIVA (proposed)
CBF	✓	wMPDR swCBF [44]	swCIVA (proposed)

separation when $M \gg N$, e.g., $M = 8$ and $N = 2$ [36].

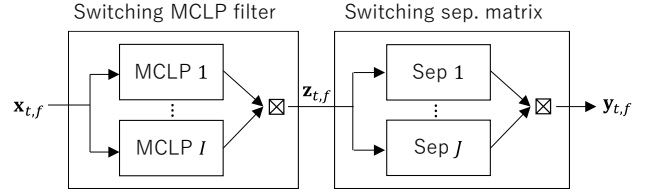
A. Problems to be solved and contributions in this paper

Despite the success of the IVA/CIVA approaches, achieving high estimation accuracy is still challenging when using a small number of microphones in the presence of diffuse noise. Currently, the performance largely degrades as the number of microphones M or more specifically $M - N$ decreases. This severely limits the application area of IVA/CIVA because use of many microphones is usually not acceptable in practical applications.

Recently, a promising algorithm to achieve higher estimation accuracy with a small number of microphones, called Minimum Variance Distortionless Response (MVDR) switching BeamFormer (swBF) [43], has been proposed as an extension of conventional MVDR BeamFormer (BF) [39], [45]. MVDR swBF is composed of a set of time-invariant BFs and a switch, and the switch selects one of the BF outputs at each time frame that the most accurately estimates the target signal. It relies on sparseness property of sources, i.e., sources are sparsely distributed in the STFT domain. With the property, the number of sources at each time-frequency (TF) point can be smaller than their total number over all TF points, and thus we can perform better beamforming by appropriately switching the BFs. The BFs and the switch are jointly optimized as those minimizing the noise power in the observed signal under a distortionless constraint with given acoustic transfer functions (ATFs) from sources to microphones. The effectiveness of WPE with the switching mechanism, called swWPE, has also been confirmed [42]. It consistently outperformed conventional WPE in diffuse noise environments and/or with underdetermined conditions. Weighted Minimum Power Distortionless Response (wMPDR) CBF with the switching mechanism [44], called wMPDR swCBF, has also been shown to outperform conventional wMPDR CBF [41].

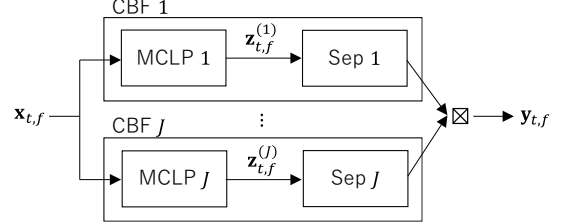
In this paper, we propose two new methods, *switching IVA* (swIVA) and *switching CIVA* (swCIVA), by incorporating the switching mechanism, respectively, into IVA and CIVA,¹ aiming at improving their performance when using a small number of microphones. We show that the optimization algorithm can be derived under the same assumptions as those used for IVA and CIVA, and all the filter coefficients and switches are jointly optimized based on the maximum-likelihood (ML)

¹It is straightforward to further incorporate IVE into swIVA/swCIVA, but this paper skips it for conciseness.



⊗ : a switch that selects an input at each time frame

(a) Factorized switching model of a swCBF, composed of a switching MCLP filter and a switching separation matrix.



(b) Direct switching model of a swCBF, composed of a set of CBFs followed by a switch.

Fig. 1. Examples of a swCBF optimized by swCIVA.

estimation. Based on our best knowledge, this is the first paper that introduces the switching mechanism into BSS. Table I summarizes taxonomy of conventional and proposed algorithms for dereverberation, beamforming, and convolutional beamforming.

Furthermore, this paper proposes several important techniques for swIVA and swCIVA to make them work appropriately. First, we introduce a *factorized switching model* shown in Fig. 1 (a) into swCBF that is optimized by swCIVA. It uses two different switches for MCLP filters and separation matrices, respectively. As will be discussed in section II-C and shown in experiments (section IV-E), this model is advantageous to capture two different time-varying characteristics of the observed signal, respectively, for dereverberation and source separation. This is not the case with a direct switching model shown in Fig. 1 (b), which uses a single switch for both dereverberation and source separation.

The second important technique is *separation matrix-wise switching* for swIVA. With a conventional swCBF [44], individual sources are estimated separately by different swBFs, each of which independently selects one of its BFs for the estimation at each time frame. In contrast, the new switching mechanism selects one of separation matrices, each of which estimates all the sources at once at each time frame, as shown in right half of Fig. 1 (a). It allows us to use computationally efficient optimization techniques proposed for conventional IVA [6], [46]–[48] also for swIVA.

Thirdly, we introduce an important heuristic into swIVA and swCIVA regarding selection of a statistical source model. Although a frequency-dependent source model is advantageous for WPE and for the optimization of the switches, a frequency-independent source model is essential for IVA. To solve this discrepancy, we introduce a hybrid source model, referred to as a *coarse-fine source model*. With the model, we use a frequency-independent model to update the separation

matrix and use a frequency-dependent model to update the other parameters, including the switch.

Finally, we design two effective initialization techniques for separation matrices of swIVA. As will be shown in our experiments, simple initialization that is often used for conventional IVA does not work well for swIVA. It is partly because sources are estimated using different separation matrices at individual switching states with swIVA, and thus they may be permuted at different states. We call this an inter-state permutation problem. To solve the problem, we propose 1) *blind single-state initialization* and 2) *spatially guided initialization*. The former allows us to optimize swIVA and swCIVA by fully blind processing. The latter, on the other hand, uses a TF mask-based BF estimated, e.g., using a neural network (NN) [41] to initialize separation matrices. The spatial guide not only solves the inter-state permutation, but also improve the optimization to converge to better stationary points [49].

In experiments, we evaluate swIVA/swCIVA in terms of signal distortion reduction and ASR improvement using 2-channel and 3-channel noisy reverberant speech mixtures. We first show that the above proposed techniques are all essential for swIVA and swCIVA to perform effective estimation. With these techniques, the switching mechanism largely improves the performance of swIVA and swCIVA. Improvement is substantial and consistent under all experimental conditions when increasing the number of switching states from one (i.e., IVA or CIVA) to two (i.e., swIVA or swCIVA) for both the separation matrices and the MCLP filters, although it becomes less stable when further increasing the number of states.

In the remainder of this paper, section II presents formulation of swIVA/swCIVA. In sections III, we describe effective initialization techniques for them. Experiments and concluding remarks are given in Sections IV and V.

II. FORMULATION OF SWIVA/SWCIVA

This section formulates swIVA/swCIVA by introducing a switching mechanism into IVA/CIVA. First, we develop swCIVA as an integrated method that includes swIVA as a processing block. Then, section II-I presents the formulation of swIVA (when solely used not integrated with swWPE) by summarizing its difference from swCIVA.

A. Model of observed signal for swCIVA

Suppose that N speech signals are captured by M distant microphones with reverberation and background diffuse noise. We assume $M \geq N$ in this paper. Let $x_{m,t,f}$ be the captured signal at the m th microphone and a TF point (t, f) in the STFT domain for $1 \leq t \leq T$ and $1 \leq f \leq F$, where T and F are the numbers of time frames and frequency bins, and let $(\cdot)^\top$ denote a non-conjugate transpose. Then the captured signal at all the microphones, $\mathbf{x}_{t,f} = [x_{1,t,f}, \dots, x_{M,t,f}]^\top \in \mathbb{C}^M$, is modeled by

$$\mathbf{x}_{t,f} = \sum_{n=1}^N \mathbf{d}_{n,t,f} + \sum_{n=1}^N \mathbf{l}_{n,t,f} + \mathbf{v}_{t,f}, \quad (1)$$

$$\mathbf{d}_{n,t,f} = \mathbf{h}_{n,f} s_{n,t,f} \quad \text{for all } n, \quad (2)$$

where $\mathbf{d}_{n,t,f} = [d_{n,1,t,f}, \dots, d_{n,M,t,f}]^\top \in \mathbb{C}^M$ is the direct signal plus the early reflections of the n th source [50], [51], $\mathbf{l}_{n,t,f}$ is the source's late reverberation, and $\mathbf{v}_{t,f}$ is the diffuse noise. This paper deals with $\mathbf{d}_{n,t,f}$ for each n as a signal to be estimated, called a desired signal, and models it by a product of a time-invariant ATF $\mathbf{h}_{n,f} \in \mathbb{C}^M$ and the n th clean source signal $s_{n,t,f} \in \mathbb{C}$ in Eq. (2).

B. Issues in conventional CIVA

To perform BSS and BD, conventional CIVA assumes determined conditions,² where the captured signal contains only point sources, and the number of sources is equal to the number of microphones. This has substantial mismatch with the above observed signal model. Diffuse noise comes to microphones from arbitrary directions, and thus is better modeled to be composed of many sources. Accordingly, in order to formulate CIVA, we need to further simplify the observation model, that is, we model it to be composed of N speech sources and $M - N$ noise components [16]. In practice, this simplification works well when $M \gg N$ (e.g., $M = 8$ and $N = 2$) and the noise level is moderate.

With the above simplification, CIVA applies a CBF to the observed signal as

$$\mathbf{y}_{t,f} = \begin{bmatrix} \mathbf{W}_f \\ \bar{\mathbf{W}}_f \end{bmatrix}^H \begin{bmatrix} \mathbf{x}_{t,f} \\ \bar{\mathbf{x}}_{t,f} \end{bmatrix} \in \mathbb{C}^M, \quad (3)$$

$$\bar{\mathbf{x}}_{t,f} = [\mathbf{x}_{t-D,f}^\top, \dots, \mathbf{x}_{t-L+1,f}^\top]^\top \in \mathbb{C}^{M(L-D)},$$

where $(\cdot)^H$ is an Hermitian transpose, and $\mathbf{W}_f \in \mathbb{C}^{M \times M}$ and $\bar{\mathbf{W}}_f \in \mathbb{C}^{M(L-D) \times M}$ are the CBF's coefficient matrices applied to the current captured signal $\mathbf{x}_{t,f}$ and the past captured signal sequence $\bar{\mathbf{x}}_{t,f}$. With a CBF, $\bar{\mathbf{W}}_f$ is introduced to appropriately handle reverberation that is longer than an analysis window. $\mathbf{y}_{t,f} = [y_{1,t,f}, \dots, y_{M,t,f}]^\top \in \mathbb{C}^M$ is the output of the CBF, including N signals corresponding to estimates of the desired signals at the reference channel [53], i.e., $d_{n,r,t,f}$ for $1 \leq n \leq N$, letting r be the index of the reference channel. The other M signals in $\mathbf{y}_{t,f}$ correspond to estimated noise components. D (≥ 1) is prediction delay introduced to set the dereverberation goal to reduce only the late reverberation and preserve the desired signals [17].

Although the observed signal can be well dereverberated and separated into N speech signals and $M - N$ noise components when $M \gg N$, the estimation becomes challenging as $M - N$ becomes small and/or the noise level becomes large. A relatively high level noise and large estimation errors remain in the separated speech signals, and dereverberation capability is seriously degraded. This problem severely limits the applicability of CIVA especially when the number of available microphones is small (e.g., 2 or 3).

C. Motivation of introducing a switching mechanism

The main aim of introducing a switching mechanism into CIVA is to reduce the above mismatch and to improve the

²To be strict, an MCLP filter requires overdetermined conditions, where microphones outnumber point sources, for performing precise dereverberation according to the multiple-input/output inverse theorem (MINT) [52].

estimation accuracy, especially when using a relatively small number of microphones. Our expectation is that the mismatch could be reduced by clustering time frames of an observed signal into several groups so that each group better fits the assumed observation model with given set of microphones. Then, each group with reduced mismatch could be more accurately handled by a conventional CBF. In general, signal components included in an observed signal, such as speech signals and their reverberation, are highly time-varying, and active components rapidly change in a frame-by-frame manner. Therefore, adaptively changing filter coefficients so that they well fit active components at each TF point can be advantageous over conventional approaches that use a fixed filter coefficients to handle all the signal components over time at once. The switching mechanism performs such adaptive processing by clustering time frames of an observed signal into groups with reduced mismatch, and applying a conventional CBF individually to each of the groups.

Let us present two examples that explain how the switching mechanism could work to reduce the mismatch. First, a speech signal is known to have a sparseness property, i.e., energy of a speech signal is sparsely distributed in the STFT domain, and different signals rarely overlap on each TF point. According to this property, the clustering may be performed to reduce the number of sources, N , included in each group [43], and thus an increased signal space, $M - N$, can be used for improving the separation of diffuse noise in each group. Next, for dereverberation, as will be described in the following subsections, prediction matrices are used to predict late reverberation included in each time frame from a past observed signal sequence. In a diffuse noise environment, the prediction matrices also need to reduce influence of the noise in the past observed signal sequence on the prediction [17]. Because such influence can be highly time-varying, the prediction matrices that optimally reduce the influence should also be time-varying. With the switching mechanism, such time-varying prediction matrices could be realized by clustering the observed signal considering the influence of the noise, and applying different sets of prediction matrices, respectively, to the clustered groups.

D. Definition of swCBF

Before deriving swCIVA, this subsection first defines structure of a CBF with switching mechanism, i.e., a swCBF.

We start by defining a time-varying CBF, and then modify it to a swCBF. A time-varying CBF is defined simply by letting coefficient matrices of a CBF in Eq. (3) time-varying as

$$\mathbf{y}_{t,f} = \begin{bmatrix} \mathbf{W}_{t,f} \\ \bar{\mathbf{W}}_{t,f} \end{bmatrix}^H \begin{bmatrix} \mathbf{x}_{t,f} \\ \bar{\mathbf{x}}_{t,f} \end{bmatrix} \in \mathbb{C}^M, \quad (4)$$

where $\mathbf{W}_{t,f}$ and $\bar{\mathbf{W}}_{t,f}$ are time-varying CBF coefficients. Then, similar to a conventional CBF [28], [34], [37], we define a factorized form of the time-varying CBF as

$$\begin{bmatrix} \mathbf{W}_{t,f} \\ \bar{\mathbf{W}}_{t,f} \end{bmatrix} = \begin{bmatrix} \mathbf{I}_M \\ -\mathbf{G}_{t,f} \end{bmatrix} \mathbf{W}_{t,f}, \quad (5)$$

where $\mathbf{G}_{t,f} \in \mathbb{C}^{M(L-D) \times M}$ is a coefficient matrix that satisfies $\bar{\mathbf{W}}_{t,f} = -\mathbf{G}_{t,f} \mathbf{W}_{t,f}$, and $\mathbf{I}_M \in \mathbb{R}^{M \times M}$ is an identity matrix. Using this factorization, $\mathbf{y}_{t,f}$ in Eq. (4) is obtained as

$$\mathbf{z}_{t,f} = \mathbf{x}_{t,f} - \mathbf{G}_{t,f}^H \bar{\mathbf{x}}_{t,f}, \quad (6)$$

$$\mathbf{y}_{t,f} = \mathbf{W}_{t,f}^H \mathbf{z}_{t,f}, \quad (7)$$

where Eq. (6) is an MCLP filter yielding a dereverberated signal $\mathbf{z}_{t,f}$ from $\mathbf{x}_{t,f}$ using a prediction matrix $\mathbf{G}_{t,f}$ and Eq. (7) is a separation matrix $\mathbf{W}_{t,f}$ that extracts $\mathbf{y}_{t,f}$ from $\mathbf{z}_{t,f}$. Eqs. (6) and (7) corresponds to filters used by swWPE and swIVA, respectively.

Because the above time-varying CBF is so flexible that over-fitting to the observed signal can easily happen, we need to introduce certain constraints to avoid it. For this purpose, we introduce a switching mechanism, called a factorized switching model in Fig. 1 (a), into the MCLP filter and the separation matrix. They are composed of a set of time-invariant MCLP filters and separation matrices, which are controlled by respective switches. We mathematically model them by sums of the time-invariant coefficient matrices with switching weights as

$$\mathbf{G}_{t,f} = \sum_{i=1}^I \gamma_{t,f}^{(i)} \mathbf{G}_f^{(i)} \quad \text{and} \quad \mathbf{W}_{t,f} = \sum_{j=1}^J \delta_{t,f}^{(j)} \mathbf{W}_f^{(j)}, \quad (8)$$

$$\gamma_{t,f}^{(i)} \in \{0, 1\}, \quad \delta_{t,f}^{(j)} \in \{0, 1\}, \quad \sum_{i=1}^I \gamma_{t,f}^{(i)} = 1, \quad \sum_{j=1}^J \delta_{t,f}^{(j)} = 1, \quad (9)$$

where I and J are the numbers of the switching states of the MCLP filter and the separation matrix, $\mathbf{G}_f^{(i)}$ for $1 \leq i \leq I$ is a prediction matrix of the i th time-invariant MCLP filter, $\mathbf{W}_f^{(j)}$ for $1 \leq j \leq J$ is the j th time-invariant separation matrix, and $\{\gamma_{t,f}^{(i)}\}_{i,t,f}$ and $\{\delta_{t,f}^{(j)}\}_{j,t,f}$ are their time-varying switching weights. In this paper, for brevity, we only consider hard switches, and allow $\gamma_{t,f}^{(i)}$ and $\delta_{t,f}^{(j)}$ to take only binary values, 0 or 1.

Based on Eqs. (6), (7), and (8), the output of swCBF $\mathbf{y}_{t,f}$ can be further rewritten as

$$\mathbf{z}_{t,f}^{(i)} = \mathbf{x}_{t,f} - (\mathbf{G}_f^{(i)})^H \bar{\mathbf{x}}_{t,f}, \quad (10)$$

$$\mathbf{y}_{t,f}^{(j)} = (\mathbf{W}_f^{(j)})^H \mathbf{z}_{t,f}^{(i)}, \quad (11)$$

$$\mathbf{y}_{t,f} = \sum_{i=1}^I \sum_{j=1}^J \beta_{t,f}^{(i,j)} \mathbf{y}_{t,f}^{(i,j)}, \quad (12)$$

$$\beta_{t,f}^{(i,j)} \in \{0, 1\}, \quad \sum_{i=1}^I \sum_{j=1}^J \beta_{t,f}^{(i,j)} = 1, \quad (13)$$

where $\beta_{t,f}^{(i,j)} = \gamma_{t,f}^{(i)} \delta_{t,f}^{(j)}$ is a unified switching weight, taking a binary value, 0 or 1. We call this an expanded form of a swCBF. Figure 2 also illustrates the structure of the form. In the following, we use this form for the derivation of the optimization algorithm.

One may consider another naive structure of a swCBF, called a direct switching model and shown in Fig. 1 (b).³

³Because a swCBF with the direct switching model can also be represented by the expanded form, the optimization algorithm developed in this paper can be applied also to it.

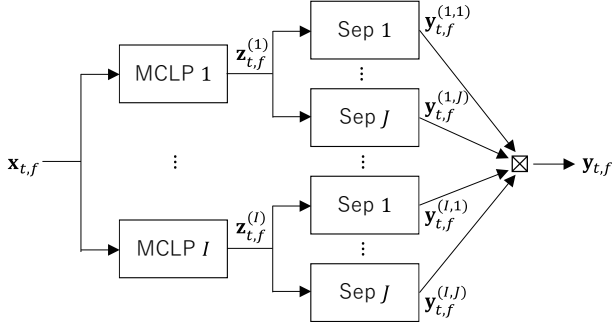


Fig. 2. An expanded form of a swCBF. Separation matrices (Sep) labeled with the same number share the same filter coefficients.

It is composed of J CBFs and a switch that selects one of the CBF's outputs at each time frame, and each CBF may be further decomposed into a pair of an MCLP filter and a separation matrix. This model, however, is sub-optimal for swCIVA as will be shown in experiments because it cannot capture time-varying characteristics of the signals separately for dereverberation and source separation.

E. Probabilistic model for swCIVA

Now, we introduce the probabilistic models to derive the ML objective. They are equivalent to those used for CIVA. We assume that a certain desired swCBF satisfies the following conditions:

- 1) The swCBF outputs, $y_{n,t,f}$ for $1 \leq n \leq M$, $1 \leq t \leq T$ and $1 \leq f \leq F$, are mutually independent, satisfying

$$p(\{y_{n,t,f}\}_{n,t,f}) = \prod_{n=1}^M \prod_{t=1}^T \prod_{f=1}^F p(y_{n,t,f}), \quad (14)$$

- 2) Each $y_{n,t,f}$ for $1 \leq n \leq M$ can be modeled by a time-varying Gaussian with a mean zero and time-varying variance $\lambda_{n,t,f}$ as

$$p(y_{n,t,f}; \lambda_{n,t,f}) = (\pi \lambda_{n,t,f})^{-1} \exp\left(-\frac{|y_{n,t,f}|^2}{\lambda_{n,t,f}}\right). \quad (15)$$

Note that here we adopt the frequency-independent source model in Eq. (15), although it is not useful for IVA to solve the well-known frequency permutation problem. Instead, this paper later introduces a frequency-dependent source model as a technique to solve the frequency permutation problem by IVA in section II-G.

Based on Eq. (4) and the above two models, we obtain the log likelihood function for a time-varying CBF to be maximized for the ML estimation of swCIVA, disregarding constant terms, as

$$\begin{aligned} \mathcal{L}(\theta) = & - \sum_{n=1}^M \sum_{t=1}^T \sum_{f=1}^F \left(\frac{|y_{n,t,f}|^2}{\lambda_{n,t,f}} + \log \lambda_{n,t,f} \right) \\ & + 2 \sum_{t=1}^T \sum_{f=1}^F \log \det |\mathbf{W}_{t,f}|, \end{aligned} \quad (16)$$

where $\theta = \{\{\lambda_{n,t,f}\}_{n,t,f}, \{\mathbf{W}_{t,f}\}_{t,f}, \{\bar{\mathbf{W}}_{t,f}\}_{t,f}\}$, and $y_{n,t,f}$ is the n th element of $\mathbf{y}_{t,f}$ in Eq. (4) obtained dependent on $\mathbf{W}_{t,f}$ and $\bar{\mathbf{W}}_{t,f}$.

Finally, with the expanded form defined by Eqs. (10) to (12), the likelihood function of swCIVA can be written as

$$\mathcal{L}(\mathcal{G}, \mathcal{W}, \Lambda, \mathcal{B}) = \sum_{t,f,i,j} \beta_{t,f}^{(i,j)} \mathcal{L}_{t,f}^{(i,j)} \left(\mathbf{G}_f^{(i)}, \mathbf{W}_f^{(j)}, \Lambda_{t,f} \right), \quad (17)$$

$$\begin{aligned} \mathcal{L}_{t,f}^{(i,j)} \left(\mathbf{G}_f^{(i)}, \mathbf{W}_f^{(j)}, \Lambda_{t,f} \right) = & - \sum_{n=1}^M \left(\frac{|y_{n,t,f}^{(i,j)}|^2}{\lambda_{n,t,f}} + \log \lambda_{n,t,f} \right) \\ & + 2 \log \det |\mathbf{W}_f^{(j)}|, \end{aligned} \quad (18)$$

where $y_{n,t,f}^{(i,j)}$ is the n th element of $\mathbf{y}_{t,f}^{(i,j)}$ obtained by Eqs. (10) and (11) dependent on $\mathbf{G}_f^{(i)}$ and $\mathbf{W}_f^{(j)}$, $\mathcal{G} = \{\mathbf{G}_f^{(i)}\}_{i,f}$, $\mathcal{W} = \{\mathbf{W}_f^{(j)}\}_{j,f}$, $\Lambda = \{\Lambda_{t,f}\}_{t,f}$, $\Lambda_{t,f} = \{\lambda_{n,t,f}\}_n$, and $\mathcal{B} = \{\beta_{t,f}^{(i,j)}\}_{i,j,t,f}$.

F. Optimization algorithm swCIVA

We now derive the algorithm, swCIVA, that optimizes a swCBF defined by Eqs. (10), (11), and (12) based on the ML objective defined by Eqs. (17) and (18).

Because no closed form solution has been obtained for the optimization, we use iterative estimation based on a coordinate ascent method [54]. It updates each parameter subset alternately by fixing the other parameter subsets, and iterates the update until convergence is obtained. The following describes each update step in the iteration.

1) *Update of \mathcal{G}* : First, extracting the terms related with $\mathbf{G}_f^{(i)}$ from Eqs. (17) and (18), we obtain

$$\mathcal{L}_{\mathbf{G}_f^{(i)}} = - \sum_{n,j,t} \frac{\beta_{t,f}^{(i,j)}}{\lambda_{n,t,f}} \left| \left(\mathbf{w}_{n,f}^{(j)} \right)^H \left(\mathbf{x}_{t,f} - \left(\mathbf{G}_f^{(i)} \right)^H \bar{\mathbf{x}}_{t,f} \right) \right|^2, \quad (19)$$

where $\mathbf{w}_{n,f}^{(j)}$ is the n th column of $\mathbf{W}_f^{(j)}$. Since the above equation is a simple quadratic form in terms of $\mathbf{G}_f^{(i)}$, we can obtain a closed form solution for it when fixing the other parameters. Let $\mathbf{g}_f^{(i)} = \text{vec}(\mathbf{G}_f^{(i)})$, where $\text{vec}(\mathbf{A})$ is an operation to reshape a matrix $\mathbf{A} = [\mathbf{a}_1, \dots, \mathbf{a}_M]$ to a vector $\mathbf{a} = [\mathbf{a}_1^T, \dots, \mathbf{a}_M^T]^T$. Then the solution is given by

$$\mathbf{g}_f^{(i)} \leftarrow \left(\Psi_f^{(i)} \right)^{-1} \text{vec}(\Phi_f^{(i)}) \in \mathbb{C}^{M^2(L-D)}. \quad (20)$$

where $(\cdot)^{-1}$ denotes a matrix inversion. $\Psi_f^{(i)} \in \mathbb{C}^{M^2(L-D) \times M^2(L-D)}$ and $\Phi_f^{(i)} \in \mathbb{C}^{M(L-D) \times M}$ are calculated as

$$\Psi_f^{(i)} = \sum_{j=1}^J \sum_{n=1}^M \left(\mathbf{w}_{n,f}^{(j)} \left(\mathbf{w}_{n,f}^{(j)} \right)^H \right)^* \otimes \mathbf{R}_{n,f}^{(i,j)}, \quad (21)$$

$$\Phi_f^{(i)} = \sum_{j=1}^J \sum_{n=1}^M \mathbf{P}_{n,f}^{(i,j)} \left(\mathbf{w}_{n,f}^{(j)} \left(\mathbf{w}_{n,f}^{(j)} \right)^H \right), \quad (22)$$

where $(\cdot)^*$ is a complex conjugate, \otimes is a Kronecker product, and $\mathbf{R}_{n,f}^{(i,j)} \in \mathbb{C}^{M(L-D) \times M(L-D)}$ and $\mathbf{P}_{n,f}^{(i,j)} \in \mathbb{C}^{M(L-D) \times M}$

are spatio-temporal covariance matrices for the n th source, which are obtained by

$$\mathbf{R}_{n,f}^{(i,j)} = \sum_{t=1}^T \frac{\beta_{t,f}^{(i,j)}}{\lambda_{n,t,f}} \bar{\mathbf{x}}_{t,f} \bar{\mathbf{x}}_{t,f}^H, \quad (23)$$

$$\mathbf{P}_{n,f}^{(i,j)} = \sum_{t=1}^T \frac{\beta_{t,f}^{(i,j)}}{\lambda_{n,t,f}} \bar{\mathbf{x}}_{t,f} \mathbf{x}_{t,f}^H. \quad (24)$$

It may be worth noting that the above update steps can be viewed as an extension of swWPE [42] using a spatial model specified by \mathcal{W} . Also, the steps follow a technique called source-wise covariance decomposition that has been proposed as a computationally efficient way to update an MCLP filter in CIVA [34].

2) *Update of \mathcal{W}* : Extracting terms related with $\mathbf{W}_f^{(j)}$ from Eqs. (17) and (18) yields

$$\mathcal{L}_{\mathbf{W}_f^{(j)}} = - \sum_{n=1}^M (\mathbf{w}_{n,f}^{(j)})^H \Sigma_{n,f}^{(j)} \mathbf{w}_{n,f}^{(j)} + 2T_f^{(j)} \log \det |\mathbf{W}_f^{(j)}|, \quad (25)$$

$$\Sigma_{n,f}^{(j)} = \sum_{i=1}^I \sum_{t=1}^T \frac{\beta_{t,f}^{(i,j)}}{\lambda_{n,t,f}} \mathbf{z}_{t,f}^{(i)} (\mathbf{z}_{t,f}^{(i)})^H, \quad (26)$$

$$T_f^{(j)} = \sum_{i=1}^I \sum_{t=1}^T \beta_{t,f}^{(i,j)}, \quad (27)$$

where $\mathbf{z}_{t,f}^{(i)}$ is the output of the i th MCLP filter in Eq. (10). Because the above objective is in the same form as that of IVA [6], we can apply iterative optimization techniques proposed for it, including Iterative Projection (IP) [6], Iterative Source Steering [46], Iterative Projection with Adjustment (IPA) [47], and accelerated AuxIVA [48]. This paper employs IP, and updates each beamformer for separating n th source for $1 \leq n \leq M$ (or the n th column of $\mathbf{W}_f^{(j)}$) as

$$\mathbf{w}_{n,f}^{(j)} \leftarrow \left((\mathbf{W}_f^{(j)})^H \Sigma_{n,f}^{(j)} \right)^{-1} \mathbf{e}_n, \quad (28)$$

$$\mathbf{w}_{n,f}^{(j)} \leftarrow \mathbf{w}_{n,f}^{(j)} / \left((\mathbf{w}_{n,f}^{(j)})^H \Sigma_{n,f}^{(j)} \mathbf{w}_{n,f}^{(j)} \right)^{1/2}, \quad (29)$$

where \mathbf{e}_n is the n th column of identity matrix \mathbf{I}_M .

3) *Updates of Λ and \mathcal{B}* : After updating $\mathbf{y}_{t,f}$ by Eqs. (11) and (12), the variance $\lambda_{n,t,f}$ is updated based on the likelihood function in Eq. (17) by the power of $y_{n,t,f}$ as

$$\lambda_{n,t,f} \leftarrow |y_{n,t,f}|^2 + \varepsilon, \quad (30)$$

where ε is a small positive scalar to avoid zero division during the optimization.

Then, according to Eq. (17), the switching weight can be updated as

$$\beta_{t,f}^{(i',j')} \leftarrow \begin{cases} 1 & \text{if } \{i', j'\} = \arg \max_{\{i,j\}} \mathcal{L}_{t,f} \left(\mathbf{G}_f^{(i)}, \mathbf{W}_f^{(j)}, \Lambda_{t,f} \right) \\ 0 & \text{otherwise.} \end{cases} \quad (31)$$

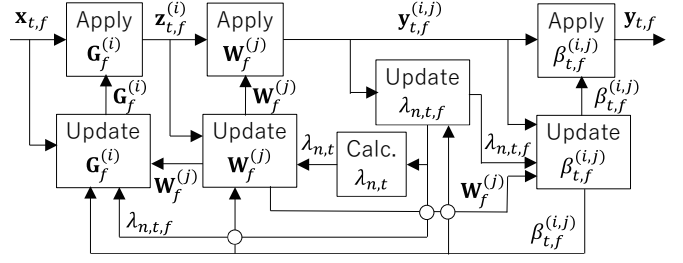


Fig. 3. Schematic diagram of swCIVA. It also becomes schematic diagram of swIVA when dropping the two blocks on \mathbf{G}_f , putting $\mathbf{x}_{t,f}$ directly into the two blocks on \mathbf{W}_f , and setting $I = 1$.

G. Introduction of coarse-fine source model

A coarse-fine source model is an important heuristic to let swCIVA work effectively. As will be shown in the experiments, the frequency-dependent source model (a fine source model) defined in Eq. (15) is essential for appropriately optimizing MCLP filters and switching weights. However, it is known that use of a frequency-independent source model (a coarse source model) is essential for IVA to effectively solve the frequency permutation problem. So, with the coarse-fine source model, we apply the coarse source model for the update of the separation matrices while using the fine source model for the other part of the optimization. The coarse source model is defined at each TF point as

$$p(y_{n,t,f}; \lambda_{n,t}) = (\pi \lambda_{n,t})^{-1} \exp \left(- \frac{|y_{n,t,f}|^2}{\lambda_{n,t}} \right), \quad (32)$$

where $\lambda_{n,t}$ is a time dependent and frequency independent variance of the n th source. Use of the coarse-fine source model has already been shown effective for the optimization of CIVA [36]. We extend the use also for the update of the switching weights in this paper.

Modification of the optimization due to the introduction of the coarse-fine source model is simple. We only need to calculate the source variances, $\lambda_{n,t}$, of the coarse source model in a step for updating separation matrices $\mathbf{W}_f^{(j)}$ by

$$\lambda_{n,t} = \frac{1}{F} \sum_{f=1}^F \lambda_{n,t,f}, \quad (33)$$

and calculate Eq. (30) using $\lambda_{n,f}$ substituted for $\lambda_{n,t,f}$.

H. Processing flow of swCIVA

Figure 3 shows the schematic diagram of swCIVA with the coarse-fine source model, and Algorithms 1, 2, and 3 summarize the processing flow that we implemented for the experiments in this paper.

As in Algorithm 1, MCLP filters, \mathcal{G} , separation matrices, \mathcal{W} , source variances, Λ , and switching weights, \mathcal{B} , are updated by iterative optimization. Line 3 corresponds to update for swWPE extended with a spatial model based on \mathcal{W} and line 4 corresponds to update for swIVA. Algorithm 2 shows the flow of updating the separation matrices in more details. Because update of the separation matrices requires more iterations until convergence than that of the MCLP filters, and the

Algorithm 1: swCIVA

Input: Observed signal $\{\mathbf{x}_{t,f}\}_{t,f}$
Output: Estimated sources $\{y_{n,t,f}\}_{1 \leq n \leq N,t,f}$

- 1 Initialize Λ , \mathcal{B} , and \mathcal{W} by Algorithm 3
- 2 **repeat**
 /* swWPE extended with \mathcal{W} */
- 3 Update \mathcal{G} and $\{\mathbf{z}_{t,f}^{(i)}\}_{i,t,f}$ by Eqs. (20)-(24) and Eq. (10)
 /* swIVA applied to $\{\mathbf{z}_{t,f}^{(i)}\}_{t,f}$ */
- 4 Update \mathcal{W} , Λ , \mathcal{B} , and $\{\mathbf{y}_{t,f}\}_{t,f}$ by Algorithm 2
- 5 **until** convergence

Algorithm 2: Update for swIVA

Input: Updated dereverberated signal $\{\mathbf{z}_{t,f}^{(i)}\}_{i,t,f}$ and variables Λ , \mathcal{B} , and \mathcal{W}
Output: Updated source estimates $\{\mathbf{y}_{t,f}\}_{t,f}$ and variables Λ , \mathcal{B} , and \mathcal{W}

- 1 **for** K times **do**
- 2 Calculate $\{\lambda_{n,t}\}_{n,t}$ by Eq. (33)
- 3 Update \mathcal{W} by Eqs. (26), (28), and (29) substituting $\lambda_{n,t,f}$ in Eq. (26) with $\lambda_{n,t}$
- 4 Update $\{\mathbf{y}_{t,f}^{(i,j)}\}_{i,j,t,f}$ and $\{\mathbf{y}_{t,f}\}_{t,f}$ by Eqs. (11) and (12)
- 5 Update Λ by Eq. (30)
- 6 Update \mathcal{B} by Eq. (31)

Algorithm 3: Simple initialization

Input: Observed signal $\{\mathbf{x}_{t,f}\}_{t,f}$
Output: Initialized Λ , \mathcal{B} and \mathcal{W}

- 1 Initialize each element of $\{\gamma_{t,f}^{(i)}\}_{i,t,f}$ and $\{\delta_{t,f}^{(j)}\}_{j,t,f}$ at a random value in a range of 1 ± 10^{-3} , and normalize it to satisfy $\sum_{i=1}^I \gamma_{t,f}^{(i)} = 1$ and $\sum_{j=1}^J \delta_{t,f}^{(j)} = 1$
 /* Iterate swWPE one time */
- 2 $\lambda_{t,f} \leftarrow \mathbf{x}_{t,f}^H \mathbf{x}_{t,f} / M + \varepsilon$ for $\{\lambda_{t,f}\}_{t,f}$
- 3 $\mathbf{R}_f^{(i)} \leftarrow \sum_t \gamma_{t,f}^{(i)} \bar{\mathbf{x}}_{t,f} \bar{\mathbf{x}}_{t,f}^H / \lambda_{t,f}$ for $\{\mathbf{R}_f^{(i)}\}_{i,f}$
- 4 $\mathbf{P}_f^{(i)} \leftarrow \sum_t \gamma_{t,f}^{(i)} \bar{\mathbf{x}}_{t,f} \mathbf{x}_{t,f}^H / \lambda_{t,f}$ for $\{\mathbf{P}_f^{(i)}\}_{i,f}$
- 5 $\mathbf{G}_f^{(i)} \leftarrow (\mathbf{R}_f^{(i)})^{-1} \mathbf{P}_f^{(i)}$ for \mathcal{G}
- 6 $\mathbf{z}_{t,f}^{(i)} \leftarrow \mathbf{x}_{t,f} - (\mathbf{G}_f^{(i)})^H \bar{\mathbf{x}}_{t,f}$ for $\{\mathbf{z}_{t,f}^{(i)}\}_{i,t,f}$
- 7 **For** $\{\gamma_{t,f}^{(i)}\}_{i,t,f}$,

$$\gamma_{t,f}^{(i)} \leftarrow \begin{cases} 1 & \text{if } i = \arg \min_{i'} |\mathbf{z}_{t,f}^{(i')}|^2 \\ 0 & \text{otherwise} \end{cases}$$
 /* Initialize swIVA by Algorithm 2 */
- 8 Initialize each element of \mathcal{W} as \mathbf{I}_M
- 9 Initialize each element of Λ as 1
- 10 $\beta_{t,f}^{(i,j)} \leftarrow \gamma_{t,f}^{(i)} \delta_{t,f}^{(j)}$ for \mathcal{B}
- 11 Update \mathcal{W} , Λ , \mathcal{B} , and $\{\mathbf{y}_{t,f}\}_{t,f}$ by Algorithm 2

computational cost of the former is much smaller than that of the latter, we iterate the update of the separation matrices K times in Algorithm 2 per an update of the MCLP filter.

Algorithm 3 shows a simple initialization scheme that corresponds to one typically used by conventional CIVA. In the algorithm, after initializing the switching weights with random variables, we apply conventional swWPE to obtain a dereverberated observed signal $\{\mathbf{z}_{t,f}^{(i)}\}_{i,t,f}$ and then update switching separation matrices K times to obtain the initial values of \mathcal{W} , Λ , and \mathcal{B} . The switching weights are first set as values between 0 and 1, and then updated to binary values during the initialization steps.

I. Formulation of swIVA

This subsection briefly presents the formulation of swIVA (not integrated with swWPE), by summarizing its difference from the formulation of swCIVA as follows.

- 1) The observation model is assumed not to include late reverberation, i.e., we set $\mathbf{I}_{n,t,f} = \mathbf{0}$ in Eq. (1).
- 2) The same issues and motivations as in sections II-B and II-C are applied except for the discussions on reverberation and dereverberation.
- 3) The definition of a switching separation matrix used for swIVA is obtained by dropping a switching MCLP filter from a swCBF, or more specifically by Eqs. (11) and (12), substituting $\mathbf{x}_{t,f}$ for $\mathbf{z}_{t,f}^{(i)}$ and setting $I = 1$.
- 4) The same assumptions as in Eqs. (14) and (15) are employed, and the same log-likelihood function as in Eqs. (17) and (18) are derived except that we drop \mathcal{G} , substitute $\mathbf{x}_{t,f}$ for $\mathbf{z}_{t,f}^{(i)}$, and set $I = 1$.
- 5) The optimization algorithm can be obtained from that of swCIVA by skipping the step updating \mathcal{G} , substituting $\mathbf{x}_{t,f}$ for $\mathbf{z}_{t,f}^{(i)}$, and setting $I = 1$.
- 6) The same coarse-fine source model is applied.

As a result, the processing flow of swIVA is obtained by modifying the Algorithms 1, 2, and 3 as follows:

- 1) All Algorithms: substitute $\mathbf{x}_{t,f}$ for $\mathbf{z}_{t,f}^{(i)}$, and let $I = 1$.
- 2) Algorithm 1: skip line 3.
- 3) Algorithm 3: skip lines 1 to 7 and initialize $\beta_{t,f}^{(1,j)}$ at line 10 following the way for initializing $\delta_{t,f}^{(j)}$ at line 1.

III. INITIALIZATION TECHNIQUES FOR SWIVA/SWCIVA

As already discussed in the introduction, the optimization of swIVA/swCIVA is sensitive to the initialization, i.e., it does not converge to good stationary points when using simple initialization in Algorithm 3. Because there is no explicit constraint on the order of estimated sources, they can be easily permuted between different switching states especially at an early stage of the optimization. We call this the inter-state permutation problem.

To solve this problem, we design two effective initialization schemes in the following: 1) blind single-state initialization and 2) spatially guided initialization. The former allows us to perform fully blind optimization, while the latter enables us to utilize spatial information obtained, e.g., by NN-based TF mask estimation.

A. Blind single-state initialization

With the blind single-state initialization, we use swIVA/swCIVA themselves for the initialization, but tentatively setting the number of switching state $J = 1$, i.e., using only one separation matrix in swIVA/swCIVA. Because swIVA/swCIVA with $J = 1$ are free from the inter-state permutation problem, we can avoid such a type of permutation errors. Note that swIVA with $J = 1$ is equivalent to IVA.

In concrete, we implement it as follows:

- 1) We start and iterate optimization of swIVA/swCIVA by setting $J = 1$ and following Algorithms 1 to 3.
- 2) After certain predetermined number of iterations, we reset the number of switching states J to its original number specified for the estimation, and re-initialize swIVA/swCIVA based on their updated parameters estimated with $J = 1$.
- 3) We continue remaining iterations for the optimization.

In our experiment, we performed the re-initialization in the above step 2 after line 1 of Algorithm 2 as

- 1) Copy the updated separation matrix, $\mathbf{W}_{t,f}^{(1)}$, to re-initialized separation matrices, $\mathbf{W}_{t,f}^{(j)}$, for $1 \leq j \leq J$.
- 2) Initialize $\delta_{t,f}^{(j)}$ at random values following line 1 of Algorithm 3, and multiply it with the updated switching weights $\beta_{t,f}^{(i,1)}$ to obtain re-initialized switching weights, $\beta_{t,f}^{(i,j)}$, for all i, j, t , and f as

$$\beta_{t,f}^{(i,j)} \leftarrow \beta_{t,f}^{(i,1)} \delta_{t,f}^{(j)}. \quad (34)$$

B. Spatially guided initialization

With this initialization, we use ATFs of the source signals separately estimated from the observed signal. It has been shown that such ATFs can be reliably estimated for conventional mask-based BFs/CBFs, e.g., using a TF mask estimation based on a neural network (NN) [41] or blind spatial clustering [21], [55]. So, we examine swIVA/swCIVA using such a technique in this paper.

In the following, we first explain how ATFs can be estimated based on TF masks, and then we describe how to initialize swIVA/swCIVA using the estimated ATFs. (See section IV-A on how we estimated the TF masks in our experiments.)

1) *TF mask-based ATF estimation*: We adopt an ATF estimation method based on the eigenvalue decomposition with noise covariance whitening [56], [57]. During the initialization step in Algorithm 3, a dereverberated observed signal $\mathbf{z}_{t,f}$ can be obtained based on swWPE after line 7 of Algorithm 3 as

$$\mathbf{z}_{t,f} = \sum_{i=1}^I \gamma_{t,f}^{(i)} \mathbf{z}_{t,f}^{(i)}. \quad (35)$$

For swIVA, we substitute $\mathbf{x}_{t,f}$ for $\mathbf{z}_{t,f}$ and set $I = 1$ in the following. Then, we estimate TF masks, $\Omega_{n,t,f}$, from $\mathbf{z}_{t,f}$ based, e.g., on a neural network. $\Omega_{n,t,f}$ takes a value between 0 and 1, where $\Omega_{n,t,f} = 1$ and 0, respectively, mean that the TF point is dominated by the n th source and dominated by the some other sources. With the masks, the covariance matrix

of the n th source, denoted by $\Gamma_{Z,n,f}$, and that of interference signals, denoted by $\Gamma_{V,n,f}$, are calculated as

$$\Gamma_{Z,n,f} = \frac{\sum_{t=1}^T \Omega_{n,t,f} \mathbf{z}_{t,f} \mathbf{z}_{t,f}^H}{\sum_{t=1}^T \Omega_{n,t,f}}, \quad (36)$$

$$\Gamma_{V,n,f} = \frac{\sum_{t=1}^T (1 - \Omega_{n,t,f}) \mathbf{z}_{t,f} \mathbf{z}_{t,f}^H}{\sum_{t=1}^T (1 - \Omega_{n,t,f})}, \quad (37)$$

Then, the ATFs can be estimated as

$$\mathbf{a}_{n,f} \leftarrow \Gamma_{V,n,f} \text{MaxEig}(\Gamma_{V,n,f}^{-1} \Gamma_{Z,n,f}), \quad (38)$$

where $\text{MaxEig}(\cdot)$ is a function to extract the eigenvector corresponding to the maximum eigenvalue.

2) *Initialization using estimated ATFs*: This technique provides a way to initialize the separation matrices \mathcal{W} and the source variances Λ , as substitution of lines 8 and 9 in Algorithm 3. First, we employ conventional Minimum Power Distortionless Response (MPDR) BF for the initialization of \mathcal{W} , where the estimated ATFs are used in the distortionless constraint, $(\mathbf{w}_{n,f}^{(j)})^H \mathbf{a}_{n,f} = a_{n,r,f}$, letting $a_{n,r,f}$ be the reference channel element of $\mathbf{a}_{n,f}$. Then, each column $\mathbf{w}_{n,f}^{(j)}$ of $\mathbf{W}_{t,f}^{(j)}$ for $1 \leq n \leq N$ and all j and f is initialized as

$$\mathbf{w}_{n,f}^{(j)} = \frac{a_{n,r,f}^* (\Xi_{n,f}^{(j)})^{-1} \mathbf{a}_{n,f}}{(\mathbf{a}_{n,f})^H (\Xi_{n,f}^{(j)})^{-1} \mathbf{a}_{n,f}}, \quad (39)$$

where $\Xi_{n,f}^{(j)}$ is a covariance matrix of $\mathbf{z}_{t,f}$. In order to generate J different sets of initial values $\mathbf{w}_f^{(j)}$ for $1 \leq j \leq J$ from the same $\mathbf{z}_{t,f}$, we introduced J different sets of time-varying frame weights $\alpha_{n,t,f}^{(j)}$ for the calculation of the covariance matrix, $\Xi_{n,f}^{(j)}$, as

$$\Xi_{n,f}^{(j)} = \frac{\sum_{t=1}^T \alpha_{n,t,f}^{(j)} \mathbf{z}_{t,f} (\mathbf{z}_{t,f})^H}{\sum_{t=1}^T \alpha_{n,t,f}^{(j)}}, \quad (40)$$

In our experiments, we randomly generate $\alpha_{n,t,f}^{(j)}$ in the same way as the initialization of $\delta_{t,f}^{(j)}$ at line 1 of Algorithm 3. As for filter coefficients to separate noise components, i.e., $\mathbf{w}_{n,f}^{(j)}$ for $N+1 \leq n \leq M$, we initialize them as $\mathbf{w}_{n,f}^{(j)} = \mathbf{e}_n$.

The variance of each source is then initialized as squared average of J BFs' outputs as

$$\lambda_{n,t,f} = \left| \frac{\sum_{j=1}^J \alpha_{n,t,f}^{(j)} (\mathbf{w}_{n,f}^{(j)})^H \mathbf{z}_{t,f}}{\sum_{j=1}^J \alpha_{n,t,f}^{(j)}} \right|^2. \quad (41)$$

IV. EXPERIMENTS

This section experimentally evaluates the performance of swIVA/swCIVA in terms of signal distortion reduction and ASR improvement. Tables II and III summarizes methods and configurations to be compared in the experiments. First, we confirm necessity of the proposed initialization techniques and the coarse-fine source model. Then, we evaluate the effect of the joint optimization in comparison with separate optimization, for which we apply conventional swWPE [42] and swIVA in a cascade configuration with no interaction. Finally, we evaluate swIVA/swCIVA with varying numbers of switching states.

TABLE II
METHODS TO BE COMPARED

Method	Switch	#States for switch(es)
IVA [6]	-	$J = 1$
swIVA	✓	$J = 2$ or 3
CIVA [32], [34]	-	$(I, J) = (1, 1)$
swCIVA	✓	$(I, J) = (1, 2), (2, 1), (2, 2), \dots$, or $(3, 3)$

TABLE III
CONFIGURATIONS TO BE COMPARED. ‘*’ INDICATES DEFAULT CONFIGURATIONS USED IN EXPERIMENTS UNLESS OTHERWISE NOTED.

Parameter	Configurations
Initialization	Simple, blind single-state, or *spatially guided
Source model	Switch: Coarse (C) or *Fine (F), MCLP: C or *F
Optimization	*Joint or separate
Switching model	*Factorized (Fig. 1 (A)) or direct (Fig. 1 (b))

A. Dataset, evaluation metrics, and analysis condition

To evaluate the estimated source signals, we used the REVERB-2MIX dataset [58], which is composed of noisy reverberant speech mixtures. Each mixture in the dataset was created by mixing two utterances (i.e., $N = 2$), extracted from the REVERB Challenge dataset (REVERB) [59], on from its development set (Dev set) and the other from its evaluation set (Eval set). REVERB-2MIX is composed of two subsets, SimuData and RealData, respectively, created from SimuData and RealData of REVERB. REVERB SimuData was generated by convolving measured impulse responses with utterances extracted from the WSJCAM0 dataset [60] and by adding measured stationary noise. The reverberant signal-to-noise (SNR) was set at 20 dB. REVERB RealData was recorded in real noisy reverberant rooms, where transcriptions of WSJCAM0 were read by humans. 8-channel data are available for REVERB-2MIX, but we only used its first 2 or 3-channels in the experiments. Following the REVERB-2MIX guideline, evaluation was performed using separated signals that correspond to Eval set of REVERB, which were selected from the estimated speech signals based on the correlation with the original signals in the REVERB Eval set.

We used the REVERB-2MIX SimuData to evaluate the distortions of enhanced signals, and used the RealData to evaluate the ASR performance of enhanced signals. As a metric to evaluate signal distortions [61], we adopted the Frequency-Weighted Segmental SNR (FWSSNR), which was shown at the REVERB challenge [59] to have relatively high correlation with subjective evaluation on perceived amount of reverberation. To evaluate the ASR performance, we calculated Word Error Rates (WERs) of enhanced signals using a baseline ASR system that was developed for REVERB using Kaldi [62]. This system is composed of a Time-Delay NN (TDNN) acoustic model trained using Lattice-Free Maximum Mutual Information (LF-MMI) and online i-vector extraction, and a trigram language model. They were trained on the REVERB training set.

We set the frame length and the shift to 32 and 8 ms and used a Hann window for the short-time analysis. The sampling frequency was 16 kHz. For an MCLP filter, the prediction delay was set at $D = 2$ and the prediction filter

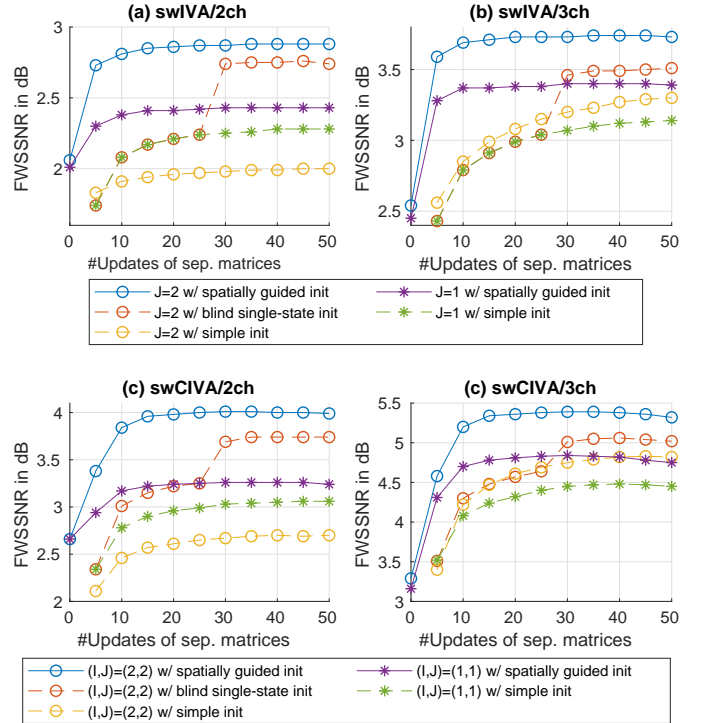


Fig. 4. FWSSNRs in dB obtained by IVA ($J = 1$), CIVA ($(I, J) = (1, 1)$), swIVA ($J = 2$), and swCIVA ($(I, J) = (2, 2)$) using spatially guided initialization, blind single-state initialization, or simple initialization. The horizontal axis indicates the number of updates of separation matrices. #updates 0 and 5, respectively, correspond to the outputs of MPDR BF used in the spatially guided initialization and the outputs of swIVA obtained after its 5 iterations in Algorithm 3. For the blind single-state initialization, we used the first 25 iterations as the initialization steps. Default configurations in Table III are used for the other parameters.

length was set at $L = 10$. For swCIVA, separation matrices were updated $K = 5$ times per one MCLP filter update, and in total separation matrices and MCLP filters were updated 50 and 10 times, respectively. We used diagonal loading for matrix inversions to make them stable in the optimization. For all the methods, we applied projection back [63] post-processing to solve scale ambiguity of BSS. For the estimation of time-frequency masks, which were used to estimate ATFs for the spatially guided initialization, we adopted a frequency-domain convolutional NN (CNN) [64] with a large receptive field, similar to the one used in a fully-Convolutional Time-domain Audio Separation Network (Conv-TasNet) [65]. We trained the CNN to estimate masks based on utterance-level permutation invariant training [66].

B. Importance of initialization

In the first experiment, we compared the performance of IVA, CIVA, swIVA and swCIVA using three types of initialization approaches, simple initialization shown in Algorithm 3, blind single-state initialization, and spatially guided initialization. Figure 4 shows FWSSNRs of enhanced signals.

First, comparing the results with swIVA ($J = 2$) and IVA ($J = 1$) in (a) and (b), swIVA greatly outperformed IVA when using the spatially guided initialization in all cases. Also, swIVA using the blind single-state initialization outperformed

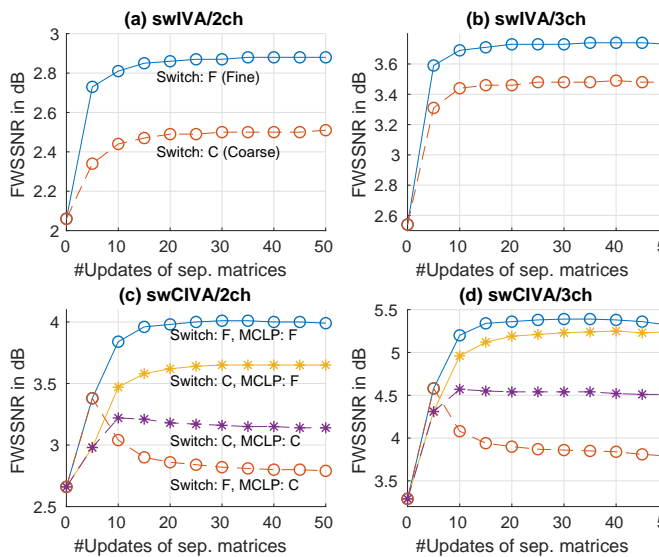


Fig. 5. FWSSNRs in dB obtained with different source models, indicated as C (Coarse) and F (Fine), for the optimization of switches (Switch) and MCLP filters (MCLP) using swIVA ($J = 2$) and swCIVA ($(I, J) = (2, 2)$). Default configurations in Table III are used for the other parameters.

IVA using the simple initialization after the initialization step finished. In contrast, swIVA underperformed IVA when using the simple initialization for the 2ch case. Next, comparing the results using swIVA ($J = 2$), the spatially guided initialization largely outperformed the others, and the blind single-state initialization was the second best. It might be worth noting that the spatially guided initialization was also very effective for IVA ($J = 1$). As for swCIVA, we can confirm the same tendency in (c) and (d).

These results clearly show the importance of the initialization for swIVA and swCIVA. Without appropriate initialization, the switching mechanism may degrade the performance. With the proposed initialization techniques, in contrast, the switching mechanism substantially and consistently improves the performance better than the case without the switching mechanism. The blind single-state initialization made swIVA and swCIVA work effectively based only on blind processing and the spatially guided initialization further improved the performance based on NN-based mask estimation.

We use the spatially guided initialization as a default configuration in Table III in the following.

C. Necessity of coarse-fine source model

Figures 5 and 6 show the FWSSNRs and WERs of the signals enhanced using swIVA/swCIVA by modifying the configuration of the source model between coarse and fine models. We set $J = 2$ for swIVA and set $(I, J) = (2, 2)$ for swCIVA. In the figure, “Switch: F” and “MCLP: F” mean that the fine source model was used, respectively, for switching weights and MCLP filters. “Switch: C” and “MCLP: C” mean that the coarse model was instead used for them. For the separation matrix, we used the coarse model in all cases.

The figures show that using the fine source model for both the switching weights and the MCLP filters greatly improved

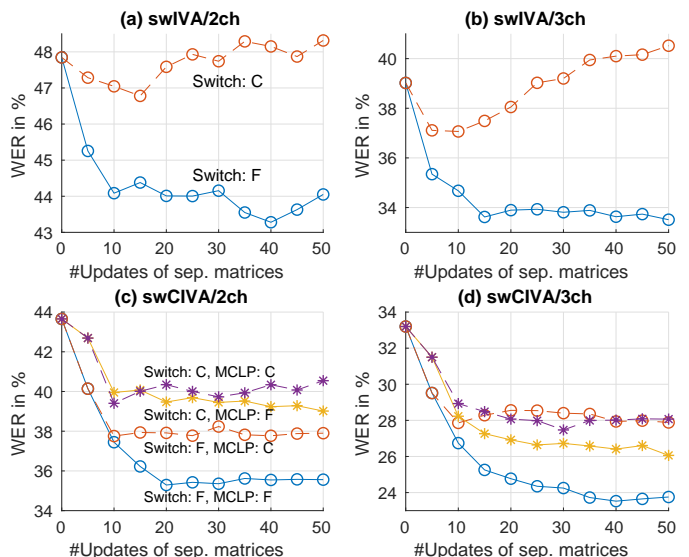


Fig. 6. WERs in % obtained with different source models, indicated as C (Coarse) and F (Fine), for the optimization of switches (Switch) and MCLP filters (MCLP) using swIVA ($J = 2$) and swCIVA ($(I, J) = (2, 2)$). Default configurations in Table III are used for the other parameters.

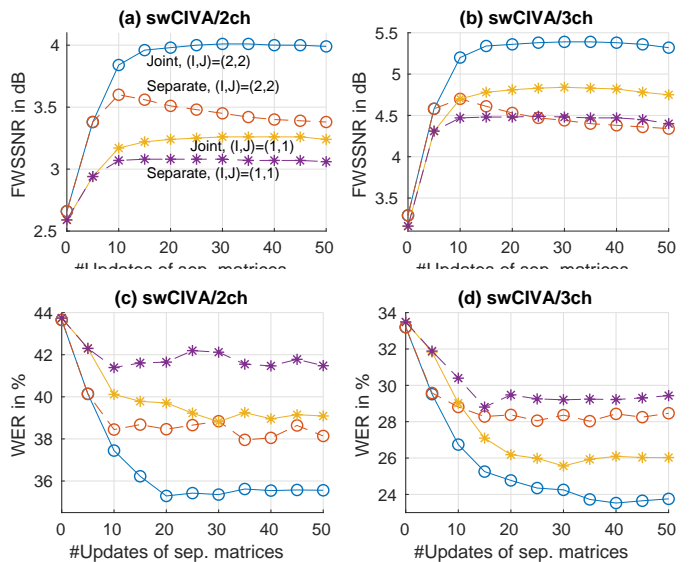


Fig. 7. FWSSNRs in dB and WERs in % obtained by CIVA ($(I, J) = (1, 1)$) and swCIVA ($(I, J) = (2, 2)$) using joint optimization (Joint) and separate optimization (Separate). Default configurations in Table III are used for the other parameters.

the performance of swIVA/swCIVA for all the cases especially in comparison with the case using the coarse model for both of them.

This result clearly shows the necessity of using coarse and fine models, respectively, for optimization of swIVA and that of MCLP filters and switches.

D. Joint optimization vs separate optimization

Next, we evaluated the effect of the joint optimization of CIVA ($(I, J) = (1, 1)$) and swCIVA ($(I, J) = (2, 2)$) in comparison with the case using the separate optimization. With the separate optimization, we connect conventional swWPE

[42] and swIVA in a cascade configuration, and optimize each of them separately with no interaction between swIVA and swWPE except for passing the output of swWPE to swIVA. The overall optimality is not guaranteed for the separate optimization.

Figure 7 shows the comparison results using 2ch/3ch observations. In all cases, the joint optimization largely outperformed the separate optimization. In particular, the joint optimization with CIVA $((I, J) = (1, 1))$ even outperformed the performance of the separate optimization with swCIVA $((I, J) = (2, 2))$ for 3-ch observation.

This result shows that the joint optimization is essential for CIVA and swCIVA.

E. Factorized switching model vs direct switching model

Figure 8 compares FWSSNRs obtained by swCIVA based on the factorized and direct switching models (Fig. 1 (a) and (b)) using 2ch and 3ch microphones. The same processing flow shown in Algorithms 1 to 3 were used with the direct switching model except that the same switch was used for MCLP filter and separation matrices. The figure shows that the factorized model $((I, J) = (2, 2))$ was substantially better than the direct model. Although the direct model improved the performance when we increased the number of switching states from $J = 1$ (i.e., conventional CIVA) to 2, further increasing the number did not improve the performance.

Figure 9 shows switching weights estimated by swCIVA with the factorized switching model $((I, J) = (2, 2))$ and the direct switching model $(J = 2)$. A spectrogram of the observed mixture is also shown. In the figure, we can clearly see different patterns in (a) and (b), i.e., switches estimated for separation matrices and MCLP filters with the factorized switching model. In contrast, the switches estimated with the direct switching model have a pattern relatively close to (a), but a bit like a mixture of (a) and (b). It may also be worth noting that (a) seems closely related with (d) the observed spectrogram structure, but we can hardly see such relationship between (b) and (d).

These results suggest that two types of the switches in swCIVA, one for MCLP filters and the other for separation matrices, capture rather different time-varying characteristics of the observed signal, and thus they play different roles. In addition, the results show the importance of the factorized switching model for making swCIVA work effectively.

F. Evaluation with various numbers of switching states

In this experiment, we varied the number of switching state for swIVA as $J = 2$ or 3 and those for swCIVA as $(I, J) = (1, 2), (2, 1), (2, 2), \dots, (3, 3)$ to examine their effect on FWSSNRs and WERs. IVA $(J = 1)$ and CIVA $((I, J) = (1, 1))$ are also compared.

Figure 10 shows FWSSNRs obtained in this case after 25 updates of the separation matrices. The figure clearly shows that FWSSNRs were consistently improved by increasing I and J , respectively, from 1 to 3. On the other hand, Fig. 11 shows WERs obtained in this experiment after 40 updates of the separation matrices. Because convergence of WERs

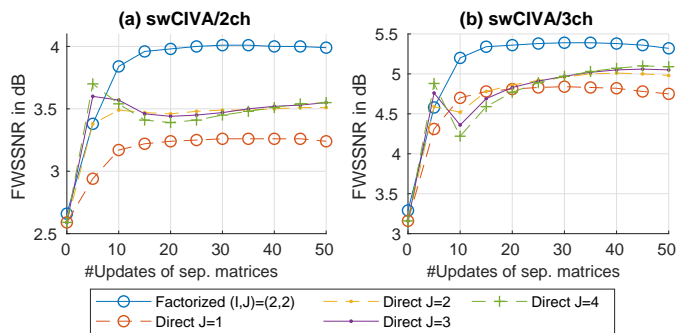


Fig. 8. FWSSNRs in dB obtained by swIVA and swCIVA using the factorized switching model $(I, J) = (2, 2)$ and the direct switching model $(J = 1, 2, 3$ and 4). Default configurations in Table III are used for the other parameters.

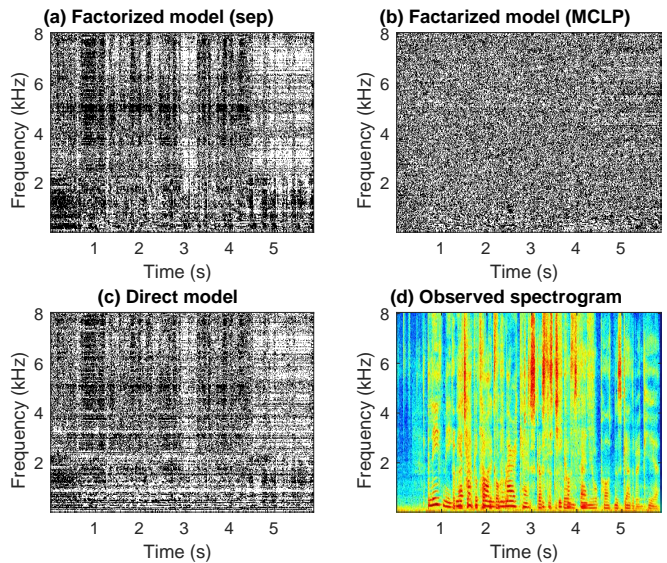


Fig. 9. Switching weights of (a) a separation matrix and (b) an MCLP filter estimated with the factorized switching model $((I, J) = (2, 2))$, (c) those estimated with the direct switching model $(J = 2)$ when using 2ch observation. Black and white at each TF point, respectively, represent a value of a switching weight, 0 and 1. Each figure shows only one of switching weights estimated for each switch. With the factorized model, switching weights of (a) a separation matrix and those of (b) an MCLP filter are calculated by $\sum_{i=1}^I \beta_{t,f}^{(i,j)}$ and $\sum_{j=1}^J \beta_{t,f}^{(i,j)}$, respectively. (d) shows a spectrogram of the observed mixture. Default configurations in Table III are used for the other parameters.

was slightly slower than that of FWSSNRs, here we show WERs obtained at a slightly late iteration step. The WERs were improved by increasing I and J from 1 to 2, but further increasing them did not necessarily improve the WERs, or even degraded them. This may be caused by overfitting of swIVA/swCIVA due to their large numbers of parameters linearly increasing as I and J increase.

These results show that swIVA and swCIVA were effective to reduce the signal distortions as well as to improve the ASR performance, but the performance becomes unstable when using large numbers of switching states.

V. CONCLUDING REMARKS

This paper proposed swIVA and swCIVA that can incorporate the switching mechanism into conventional IVA-based

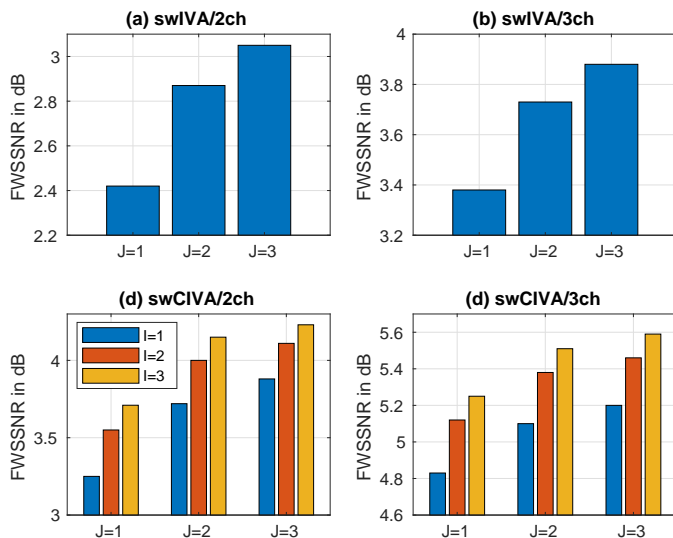


Fig. 10. FWSSNRs in dB obtained with different number of switching states using IVA ($J = 1$), CIVA ($(I, J) = (1, 1)$), swIVA ($J = 2$ or 3), and swCIVA ($(I, J) = (1, 2), (2, 1), (2, 2), \dots$, or $(3, 3)$) after 25 iterations. Default configurations in Table III are used for the other parameters.

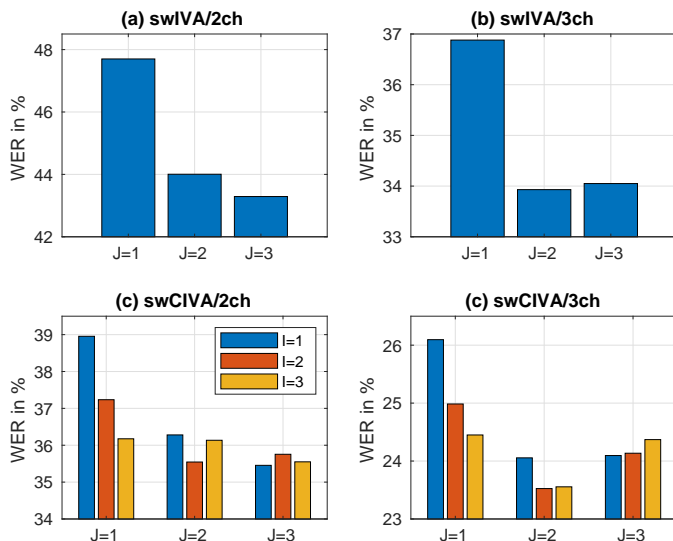


Fig. 11. WER in % obtained with different number of switching states using IVA ($J = 1$), CIVA ($(I, J) = (1, 1)$), swIVA ($J = 2$ or 3), and swCIVA ($(I, J) = (1, 2), (2, 1), (2, 2), \dots$, or $(3, 3)$) after 40 iterations. Default configurations in Table III are used for the other parameters.

source separation and CIVA-based joint source separation and dereverberation to improve their performance when only a relatively small number of microphones are available. The switching mechanism enables the improvement by clustering time frames of an observed signal into groups that can be well handled by a small number microphones, and by assigning conventional IVA/CIVA techniques to process individual groups independently. Several essential techniques were introduced to let swIVA and swCIVA work appropriately, including two initialization techniques based, respectively, on blind and spatially guided approaches, a coarse-fine source model, a factorized switching model, and a separation matrix-wise switching. Experiments showed that both swIVA and

swCIVA greatly outperformed the conventional IVA and CIVA in terms of FWSSNRs and ASR scores when using 2 or 3 microphones. In concrete, steady and substantial improvement was obtained when we set the number of switching states at two for MCLP filters and for separation matrices, respectively.

REFERENCES

- [1] J. Li, L. Deng, R. Haeb-Umbach, and Y. Gong, *Robust Automatic Speech Recognition: A Bridge to Practical Applications*. Academic Press, 2015.
- [2] P. Comon, “Independent component analysis, a new concept?” *Signal Processing*, vol. 36, no. 3, pp. 287–314, 1994.
- [3] A. Hyvärinen, J. Karhunen, and E. Oja, *Independent Component Analysis*. New York: John Wiley & Sons, 2001.
- [4] T. Kim, H. T. Attias, S.-Y. Lee, and T.-W. Lee, “Blind source separation exploiting higher-order frequency dependencies,” *IEEE Trans. Speech, and Audio Processing*, vol. 15, no. 1, pp. 70–79, 2006.
- [5] A. Hiroe, “Solution of permutation problem in frequency domain ica, using multivariate probability density functions,” in *Independent Component Analysis and Blind Signal Separation*, 2006, pp. 601–608.
- [6] N. Ono and S. Miyabe, “Auxiliary-function-based independent component analysis for super-Gaussian sources,” in *LVA/ICA*. Springer, 2010, pp. 165–172.
- [7] N. Duong, E. Vincent, and R. Gribonval, “Under-determined reverberant audio source separation using a full-rank spatial covariance model,” *IEEE Trans. Audio, Speech, and Language Processing*, vol. 18, no. 7, pp. 1830–1840, 2010.
- [8] N. Ito, R. Ikeshita, H. Sawada, and T. Nakatani, “A joint diagonalization based efficient approach to underdetermined blind audio source separation using the multichannel wiener filter,” *IEEE/ACM Trans. Audio, Speech, and Language Processing*, vol. 28, pp. 1950–1965, 2021.
- [9] H. Sawada, S. Araki, and S. Makino, “Underdetermined convolutive blind source separation via frequency bin-wise clustering and permutation alignment,” *IEEE Trans. Audio, Speech, and Language Processing*, vol. 19, no. 3, pp. 516–527, 2011.
- [10] D. H. T. Vu and R. Haeb-Umbach, “Blind speech separation employing directional statistics in an expectation maximization framework,” in *Proc. IEEE ICASSP*, 2010, pp. 241–244.
- [11] M. Souden, S. Araki, K. Kinoshita, T. Nakatani, and H. Sawada, “A multichannel MMSE-based framework for speech source separation and noise reduction,” *IEEE Trans. Audio, Speech, and Language Processing*, vol. 21, no. 9, pp. 1913–1928, 2010.
- [12] H. Sawada, S. Araki, R. Mukai, and S. Makino, “Blind extraction of a dominant source signal from mixtures of many sources,” in *Proc. IEEE ICASSP*, vol. III, 2005, pp. 61–64.
- [13] Y. Kubo, N. Takamune, D. Kitamura, and H. Saruwatari, “Efficient full-rank spatial covariance estimation using independent low-rank matrix analysis for blind source separation,” in *Proc. EUSIPCO*, 2019, pp. 1814–1818.
- [14] Z. Koldovský and P. Tichavský, “Gradient algorithms for complex non-gaussian independent component/vector extraction, question of convergence,” *IEEE Transactions on Signal Processing*, vol. 67, no. 4, pp. 1050–1064, 2018.
- [15] R. Scheibler and N. Ono, “Independent vector analysis with more microphones than sources,” in *Proc. IEEE WASPAA*, 2019.
- [16] R. Ikeshita, T. Nakatani, and S. Araki, “Block coordinate descent algorithms for auxiliary-function-based independent vector extraction,” *IEEE Trans. Signal Processing*, vol. 69, pp. 3252–3267, 2021.
- [17] T. Nakatani, T. Yoshioka, K. Kinoshita, M. Miyoshi, and B.-H. Juang, “Speech dereverberation based on variance-normalized delayed linear prediction,” *IEEE Transactions on Audio, Speech, and Language Processing*, vol. 18, no. 7, pp. 1717–1731, 2010.
- [18] T. Yoshioka and T. Nakatani, “Generalization of multi-channel linear prediction methods for blind MIMO impulse response shortening,” *IEEE Transactions on Audio, Speech and Language Processing*, vol. 20, no. 10, pp. 2707–2720, 2012.
- [19] A. Jukić, T. van Waterschoot, T. Gerkmann, and S. Doclo, “Multi-channel linear prediction-based speech dereverberation with sparse priors,” *IEEE/ACM Transactions on Audio, Speech and Language Processing*, vol. 23, no. 9, pp. 1509–1520, 2015.
- [20] T. Yoshioka and T. Nakatani, “Dereverberation for reverberation-robust microphone arrays,” in *Proc. EUSIPCO*, 2013.
- [21] N. Kanda, C. Boeddeker, J. Heitkaemper, Y. Fujita, S. Horiguchi, K. Nagamatsu, and R. Haeb-Umbach, “Guided source separation meets a strong ASR backend: Hitachi/Paderborn university joint investigation for dinner party ASR,” in *Proc. Interspeech*, 2019, pp. 1248–1252.

- [22] M. Delcroix, T. Yoshioka, A. Ogawa, Y. Kubo, M. Fujimoto, N. Ito, K. Kinoshita, M. Espi, S. Araki, T. Hori, and T. Nakatani, "Strategies for distant speech recognition in reverberant environments," *EURASIP J. Adv. Signal Process.*, vol. Article ID 2015:60, doi:10.1186/s13634-015-0245-7, 2015.
- [23] R. Haeb-Umbach, S. Watanabe, T. Nakatani, M. Bacchiani, B. Hoffmeister, M. Seltzer, H. Zen, and M. Souden, "Speech processing for digital home assistants," *IEEE Signal Processing Magazine*, vol. 36, no. 6, pp. 111–124, 2019.
- [24] M. K. Nandwana, J. van Hout, C. Richey, M. McLaren, M. A. Barrios, and A. Lawson, "The voices from a distance challenge 2019," in *Proc. Interspeech*, 2019, pp. 2438–2442.
- [25] S. Horiguchi, N. Yalta, P. Garcia, Y. Takashima1, Y. Xue, D. Raj, Z. Huang, Y. Fujita, S. Watanabe, and S. Khudanpur, "The Hitachi-JHU DIHARD III system: Competitive end-to-end neural diarization and x-vector clustering systems combined by dover-lap," *arXiv:2102.01363*, 2021.
- [26] S. Amari, S. C. Douglas, A. Cichocki, and H. H. Yang, "Multichannel blind deconvolution and equalization using the natural gradient," in *Proc. IEEE Int. Workshop on Signal Processing Advances in Wireless Communications*, 1997, pp. 101–107.
- [27] H. Buchner, R. Aichner, and W. Kellermann, "TRINICON: a versatile framework for multichannel blind signal processing," in *Proc. IEEE ICASSP*, vol. III, 2004, pp. 889–892.
- [28] T. Yoshioka, T. Nakatani, M. Miyoshi, and H. G. Okuno, "Blind separation and dereverberation of speech mixtures by joint optimization," *IEEE Trans. Audio, Speech, and Language Processing*, vol. 19, no. 1, January 2011.
- [29] M. Togami, Y. Kawaguchi, R. Takeda, Y. Obuchi, and N. Nukaga, "Multichannel speech dereverberation and separation with optimized combination of linear and non-linear filtering," in *Proc. IEEE ICASSP*, 2012, pp. 4057–4060.
- [30] H. Kagami, H. Kameoka, and M. Yukawa, "Joint separation and dereverberation of reverberant mixtures with determined multichannel non-negative matrix factorization," in *Proc. IEEE ICASSP*, 2018, pp. 31–35.
- [31] X. Li, L. Girin, S. Gannot, and R. Horaud, "Multichannel source separation and speech enhancement using the convolutive transfer function," *IEEE/ACM Trans. Audio, Speech, and Language Processing*, vol. 27, no. 3, pp. 645–659, March 2019.
- [32] R. Ikeshita, N. Ito, T. Nakatani, and H. Sawada, "Independent low-rank matrix analysis with decorrelation learning," in *Proc. IEEE WASPAA*, October 2019.
- [33] T. Dietzen, S. Doclo, M. Moonen, and T. van Waterschoot, "Integrated sidelobe cancellation and linear prediction Kalman filter for joint multi-microphone speech dereverberation, interfering speech cancellation, and noise reduction," *IEEE/ACM Trans. Audio, Speech, and Language Processing*, vol. 28, pp. 740–754, January 2020.
- [34] T. Nakatani, R. Ikeshita, K. Kinoshita, H. Sawada, and S. Araki, "Computationally efficient and versatile framework for joint optimization of blind speech separation and dereverberation," in *Proc. Interspeech*, 2020, pp. 91–95.
- [35] T. Nakashima, R. Scheibler, M. Togami, and N. Ono, "Joint dereverberation and separation with iterative source steering," in *Proc. IEEE ICASSP*, 2021.
- [36] T. Nakatani, R. Ikeshita, K. Kinoshita, H. Sawada, and S. Araki, "Blind and neural network-guided convolutional beamformer for joint denoising, dereverberation, and source separation," in *IEEE ICASSP*, 2021, pp. 6129–6133.
- [37] R. Ikeshita and T. Nakatani, "Independent vector extraction for fast joint blind source separation and dereverberation," *IEEE Signal Processing Letters*, vol. 28, pp. 972–976, 2021.
- [38] M. Togami and R. Scheibler, "Over-determined speech source separation and dereverberation," in *Proc. APSIPA*, Dec. 2020, pp. 705–710.
- [39] B. D. V. Veen and K. M. Buckley, "Beamforming: A versatile approach to spatial filtering," *IEEE ASSP Magazine*, vol. 5, no. 2, pp. 4–24, 1988.
- [40] C. Boeddeker, T. Nakatani, K. Kinoshita, and R. Haeb-Umbach, "Jointly optimal dereverberation and beamforming," in *Proc. IEEE ICASSP*, 2020.
- [41] T. Nakatani, C. Boeddeker, K. Kinoshita, R. Ikeshita, M. Delcroix, and R. Haeb-Umbach, "Jointly optimal denoising, dereverberation, and source separation," *IEEE/ACM Trans. Audio, Speech, and Language Processing*, vol. 28, pp. 2267–2282, 2020.
- [42] R. Ikeshita, N. Kamo, and T. Nakatani, "Blind signal dereverberation based on mixture of weighted prediction error models," *IEEE Signal Processing Letters*, vol. 28, pp. 399–403, 2021.
- [43] K. Yamaoka, N. Ono, S. Makino, and T. Yamada, "Time-frequency-bin-wise switching of minimum variance distortionless response beamformer for underdetermined situations," in *Proc. IEEE ICASSP*, 2019, pp. 7908–7912.
- [44] T. Nakatani, R. Ikeshita, N. Kamo, K. Kinoshita, S. Araki, and H. Sawada, "Switching convolutional beamformer," in *Proc. EUSIPCO*, 2021.
- [45] H. L. V. Trees, *Optimum Array Processing, Part IV of Detection, Estimation, and Modulation Theory*. New York: Wiley-Interscience, 2002.
- [46] R. Scheibler and N. Ono, "Fast and stable blind source separation with rank-1 updates," in *Proc. IEEE ICASSP*, 2020, pp. 236–240.
- [47] R. Scheibler, "Independent vector analysis via log-quadratically penalized quadratic minimization," *IEEE Trans. Signal Processing*, vol. 69, pp. 2509–2524, 2021.
- [48] A. Brendel and W. Kellermann, "Accelerating auxiliary function-based independent vector analysis," in *Proc. IEEE ICASSP*, 2021.
- [49] C. Boeddeker, F. Rautenberg, and R. Haeb-Umbach, "A comparison and combination of unsupervised blind source separation techniques," *arXiv:2106.05627*, 2021.
- [50] J. S. Bradley, H. Sato, and M. Picard, "On the importance of early reflections for speech in rooms," *The Journal of the Acoustic Society of America*, vol. 113, pp. 3233–3244, 2003.
- [51] T. Nishiura, Y. Hirano, Y. Denda, and M. Nakayama, "Investigations into early and late reflections on distant-talking speech recognition toward suitable reverberation criteria," in *Proc. Interspeech*, 2007, pp. 1082–1085.
- [52] M. Miyoshi and Y. Kaneda, "Inverse filtering of room acoustics," *IEEE Trans. Acoustics, Speech, and Signal Processing*, vol. 36, no. 2, pp. 145–152, 1988.
- [53] I. Cohen, "Relative transfer function identification using speech signals," *IEEE Trans. Speech, and Audio Processing*, vol. 12, no. 5, pp. 451–459, 2004.
- [54] S. J. Wright, "Coordinate descent algorithms," *Mathematical Programming*, vol. 151, no. 1, pp. 3–34, 2015.
- [55] N. Ito, S. Araki, and T. Nakatani, "Complex angular central Gaussian mixture model for directional statistics in mask-based microphone array signal processing," *Proc. EUSIPCO*, pp. 1153–1157, 2016.
- [56] S. Markovich-Golan, S. Gannot, and I. Cohen, "Multichannel eigenspace beamforming in a reverberant noisy environment with multiple interfering speech signals," *IEEE Trans. ASLP*, vol. 17, no. 6, pp. 1071–1086, 2009.
- [57] Z. Wang, E. Vincent, R. Serizel, and Y. Yan, "Rank-1 constrained multichannel Wiener filter for speech recognition in noisy environments," *Computer Speech & Language*, vol. 49, pp. 37–51, May 2018.
- [58] "REVERB-2MIX," <https://github.com/mttcslab-sp/REVERB-2MIX/>.
- [59] K. Kinoshita, M. Delcroix, S. Gannot, E. A. P. Habets, R. Haeb-Umbach, W. Kellermann, V. Leutnant, R. Maas, T. Nakatani, B. Raj, A. Sehr, and T. Yoshioka, "A summary of the REVERB challenge: State-of-the-art and remaining challenges in reverberant speech processing research," *EURASIP Journal on Advances in Signal Processing*, 2016.
- [60] T. Robinson, J. Fransen, D. Pye, J. Foote, and S. Renals, "WSJCAMO: A British English speech corpus for large vocabulary continuous speech recognition," in *Proc. IEEE ICASSP*, 1995, pp. 81–84.
- [61] Y. Hu and P. C. Loizou, "Evaluation of objective quality measures for speech enhancement," *IEEE Trans. Audio, Speech, and Language Processing*, vol. 16, no. 1, pp. 229–238, 2008.
- [62] D. Povey, A. Ghoshal, G. Boulianne, L. Burget, O. Glembek, N. Goel, M. Hannemann, P. Motlicek, Y. Qian, P. Schwarz, J. Silovsky, G. Stemmer, and K. Vesely, "The Kaldi speech recognition toolkit," in *Proc. IEEE ASRU*, 2011.
- [63] N. Murata, S. Ikeda, and A. Ziehe, "An approach to blind source separation based on temporal structure of speech signals," *Neurocomputing*, vol. 41, no. 1–4, p. 1–24, Oct. 2001.
- [64] F. Bahmaninezhad, J. Wu, R. Gu, S.-X. Zhang, Y. Xu, M. Yu, and D. Yu, "A comprehensive study of speech separation: spectrogram vs waveform separation," in *Proc. Interspeech*, 2019, pp. 4574–4578.
- [65] Y. Luo and N. Mesgarani, "Conv-TasNet: Surpassing ideal time-frequency magnitude masking for speech separation," *IEEE/ACM Trans. Audio, Speech, and Language Processing*, vol. 27, no. 8, pp. 1256–1266, 2019.
- [66] M. Kolbæk, D. Yu, Z.-H. Tan, and J. Jensen, "Multitalker speech separation with utterance-level permutation invariant training of deep recurrent neural networks," *IEEE Trans. Audio, Speech, and Language Processing*, pp. 1901–1913, 2017.